REPORT DOCUMENTATION PAGE

Form Approved
OMB No. 0704-0188

PLEASE DO NOT RETURN YOUR FORM TO THE ABOVE ADDRESS.

1. REPORT DATE *(DD-MM-YYYY)*	2. REPORT TYPE	3. DATES COVERED *(From - To)*
2008	Reprint	Aug 2007-Aug 2008

4. TITLE AND SUBTITLE

Combustion characteristics of nanoaluminum, liquid water, and hydrogen peroxide mixtures

5a. CONTRACT NUMBER

W911NF-04-1-0178

5b. GRANT NUMBER

5c. PROGRAM ELEMENT NUMBER

6. AUTHOR(S)

J.L. Sabourin a, Richard A. Yetter a, Grant A. Risha b, Steven F. Son c and B. C. Tappan d

5d. PROJECT NUMBER

5e. TASK NUMBER

5f. WORK UNIT NUMBER

7. PERFORMING ORGANIZATION NAME(S) AND ADDRESS(ES)

a The Pennsylvania State University, University Park, PA, USA
b The Pennsylvania State University—Altoona, Altoona, PA, USA
c Purdue University, West Lafayette, IN, USA
d Los Alamos National Laboratory, Los Alamos, NM, USA

8. PERFORMING ORGANIZATION REPORT NUMBER

9. SPONSORING/MONITORING AGENCY NAME(S) AND ADDRESS(ES)

U. S. Army Research Office
P.O. Box 12211
Research Triangle Park, NC 27709-2211

10. SPONSOR/MONITOR'S ACRONYM(S)

11. SPONSOR/MONITOR'S REPORT NUMBER(S)

12. DISTRIBUTION/AVAILABILITY STATEMENT

Approved for public release; federal purpose rights.

13. SUPPLEMENTARY NOTES

The views, opinions and/or findings contained in this report are those of the author(s) and should not be construed as an official

14. ABSTRACT

An experimental investigation of the combustion characteristics of nanoaluminum (nAl), liquid water (H2O(l)), and hydrogen peroxide (H2O2) mixtures has been conducted. Linear and mass-burning rates as functions of pressure, equivalence ratio (Φ), and concentration of H2O2 in H2O(l) oxidizing solution are reported. Steady-state burning rates were obtained at room temperature using a windowed pressure vessel over an initial pressure range of 0.24 to 12.4 MPa in argon, using average nAl particle diameters of 38 nm, Φ from 0.5 to 1.3, and H2O2 concentrations between 0 and 32% by mass. At a nominal pressure of 3.65 MPa, under stoichiometric conditions, mass-burning rates per unit area ranged between 6.93 g/cm2 s (0%H2O2) and 37.04 g/cm2 s (32% H2O2), which corresponded to linear burning rates of 9.58 and 58.2 cm/s, respectively. Burning rate pressure exponents of 0.44 and 0.38 were found for stoichiometric mixtures at room temperature containing 10 and 25% H2O2, respectively, up to 5MPa. Burning rates are reduced above ~5MPa due to the pressurization of interstitial spaces of the packed reactant mixture with argon gas, diluting the fuel and oxidizer mixture. Mass burning rates were not measured above ~32% H2O2 due to an anomalous burning

15. SUBJECT TERMS

Aluminum; Combustion; Water; Hydrogen peroxide; Nanoaluminum; Burning rate; Efficiency

16. SECURITY CLASSIFICATION OF:			17. LIMITATION OF ABSTRACT	18. NUMBER OF PAGES	19a. NAME OF RESPONSIBLE PERSON
a. REPORT	b. ABSTRACT	c. THIS PAGE			Richard A. Yetter
UU	UU	UU	UU	15	19b. TELEPHONE NUMBER *(Include area code)* 814-863-6375

Reset

Standard Form 298 (Rev. 8/98)
Prescribed by ANSI Std. Z39.18

Available online at www.sciencedirect.com
ScienceDirect
Combustion and Flame 154 (2008) 587–600
Combustion and Flame
www.elsevier.com/locate/combustflame

Combustion characteristics of nanoaluminum, liquid water, and hydrogen peroxide mixtures

J.L. Sabourin [a,*], G.A. Risha [b], R.A. Yetter [a], S.F. Son [c], B.C. Tappan [d]

[a] *The Pennsylvania State University, Department of Mechanical and Nuclear Engineering, University Park, PA 16801, USA*
[b] *The Pennsylvania State University, Division of Business and Engineering, Altoona, PA 16601, USA*
[c] *Purdue University, School of Mechanical Engineering, West Lafayette, IN 47907, USA*
[d] *Los Alamos National Laboratory, Los Alamos, NM 87545, USA*

Received 8 October 2007; received in revised form 20 May 2008; accepted 26 May 2008

Available online 9 July 2008

Abstract

An experimental investigation of the combustion characteristics of nanoaluminum (nAl), liquid water ($H_2O_{(l)}$), and hydrogen peroxide (H_2O_2) mixtures has been conducted. Linear and mass-burning rates as functions of pressure, equivalence ratio (Φ), and concentration of H_2O_2 in $H_2O_{(l)}$ oxidizing solution are reported. Steady-state burning rates were obtained at room temperature using a windowed pressure vessel over an initial pressure range of 0.24 to 12.4 MPa in argon, using average nAl particle diameters of 38 nm, Φ from 0.5 to 1.3, and H_2O_2 concentrations between 0 and 32% by mass. At a nominal pressure of 3.65 MPa, under stoichiometric conditions, mass-burning rates per unit area ranged between 6.93 g/cm^2 s (0% H_2O_2) and 37.04 g/cm^2 s (32% H_2O_2), which corresponded to linear burning rates of 9.58 and 58.2 cm/s, respectively. Burning rate pressure exponents of 0.44 and 0.38 were found for stoichiometric mixtures at room temperature containing 10 and 25% H_2O_2, respectively, up to 5 MPa. Burning rates are reduced above ~5 MPa due to the pressurization of interstitial spaces of the packed reactant mixture with argon gas, diluting the fuel and oxidizer mixture. Mass burning rates were not measured above ~32% H_2O_2 due to an anomalous burning phenomena, which caused overpressurization within the quartz sample holder, leading to tube rupture. High-speed imaging displayed fingering or jetting ahead of the normal flame front. Localized pressure measurements were taken along the sample length, determining that the combustion process proceeded as a normal deflagration prior to tube rupture, without significant pressure buildup within the tube. In addition to burning rates, chemical efficiencies of the combustion reaction were determined to be within approximately 10% of the theoretical maximum under all conditions studied.

Keywords: Aluminum; Combustion; Water; Hydrogen peroxide; Nanoaluminum; Burning rate; Efficiency

1. Introduction

The combustion of metals with various oxidizers has been an area of great interest for decades due to their inherent thermodynamic advantages. Metal particles by and large possess high heats of combus-

* Corresponding author. Fax: +1 (814) 865 3389.
E-mail address: jls861@psu.edu (J.L. Sabourin).

0010-2180/$ – see front matter
doi:10.1016/j.combustflame.2008.05.015

tion and favorable densities, thereby enabling large energy release per unit volume. Aluminum (Al) has historically been the primary metal of interest due to its desirable properties: abundance, insensitivity, and the stability of reaction products formed, allowing for maximum heat release. Typically, fundamental studies of Al particle combustion have involved gaseous oxidizers such as O_2, CO, CO_2, and H_2O [1–5], but there has been little work devoted to liquid oxidizer systems.

The majority of the fundamental work published to date on Al–liquid oxidizer systems has focused on using liquid water. The earlier work used Al films [6] or micrometer-sized Al particles [7–9]; however, as manufacturing technologies have progressed, nanoaluminum (nAl) particles have been used [10–15]. Ivanov et al. [7,8] investigated the effect of pressure on ultrafine metal aluminum powders in a mixture of water combined with a thickening agent, polyacrylamide (3%). It was reported that the mixture would not self-deflagrate without the addition of the thickening agent into the mixture. At their maximum test pressure, 7 MPa, the maximum linear burning rate (r_b) achieved was approximately 1.5 cm/s. There was no report of packing densities; therefore, mass-burning rates (m_b) could not be determined. Shafirovich et al. [10] used 80-nm Al–liquid water mixtures, also with a polyacrylamide gelling agent, determining combustion efficiency to be approximately 50%, while in our other study [15], combustion efficiencies of greater than 85% were obtained using 38-nm Al–$H_2O_{(l)}$ mixtures without the use of a gelling agent.

The size and shape of metallic fuel particles play a major role in their combustion. Nanoscale metallic fuel particles offer several significant advantages over micrometer- and larger-sized particles, including reduced melting temperatures, combustion times, ignition temperatures, and ignition delays. These differences are attributed to the fact that reducing particle size increases the surface-to-bulk-atom ratio and the specific surface area of the particles, affecting thermodynamic and heat transfer characteristics. The shortened burning times (t_b), described by the d^2-law of diffusion flame theory ($t_{b,diff} \propto d_p^2$) and the d^1-law for kinetically limited combustion ($t_{b,kin} \propto d_p$), allow more complete combustion in volume-limited systems, increasing chemical efficiencies. The effect of particle diameter on linear and mass-burning rates of a 38-nm Al–liquid H_2O system was studied previously. It was observed that burning rates per unit area were inversely proportional to diameter (d_p^{-1}) [14,15]. This indicates a diffusion-limited process, since $r_b \propto RR^{1/2} \propto t_b^{-1/2} \propto d_p^{-1}$. However, these studies were performed at nominal pressures greater than 0.5 MPa; at lower pressures, kinetically limited combustion is expected to occur, altering the burning rate dependence. This study was also conducted using only three particle diameters, limiting the accuracy of the derived fit.

The high specific surface areas of nanoscale particles also increase adsorption of liquid oxidizers, allowing the fuel to act as a gelling agent, reducing the need for inert additives traditionally used to gel liquids such as metal oxides. There are some drawbacks, however, to the use of smaller particles, particularly with metal particles that possess an oxide passivation layer, such as aluminum. Aluminum particles generally have an inert oxide (alumina) passivation layer 2–5 nm thick. This layer serves an important purpose, providing the particle with chemical stability under normal handling and storage conditions; however, the inert nature of the oxide layer reduces energy densities. For nanoscale particles, this layer becomes a significant portion of overall particle mass, reducing overall heat of reaction per unit mass and volume. There are several research efforts under way to reduce or replace this layer with more energetically favorable coatings using improved manufacturing technologies [16–19], but this problem has proven difficult to resolve. The primary problem involves maintaining a passivated particle that may be stored in oxygen-containing environments for extended periods of time without significant reaction, while increasing the overall energy density. Research has also shown that combustion rates and chemical conversion efficiencies are sensitive to particle shape as well. Eapen et al. have shown experimentally that aerosolized spherical aluminum particles in air react faster and more efficiently than flake aluminum, even at high “BET diameters” [20].

Hydrogen peroxide (H_2O_2) is a highly reactive and storable energetic liquid oxidizer that has been applied to many combustion applications. Prior to and during World War II, German scientists demonstrated the use of H_2O_2 in catalytically initiated reactions for submarine, torpedo, and rocket propulsion, as well as auxiliary power sources [21]. Since World War II, most combustion studies involving H_2O_2 have focused on the performance characteristics of hybrid rocket engines, using solid or liquid fuels and high test peroxide (HTP, $\geqslant$85% H_2O_2) as the oxidizer [22–26]. Problems with the use of H_2O_2 systems include its sensitivity to shock and its tendency to decompose, usually as a consequence of minute contamination; when lower concentrations are used this problem is not significant.

In the present research, the nAl–liquid water system has been investigated further by adding H_2O_2 to the reactants in order to increase chemical heat release while maintaining the same “green” reaction products

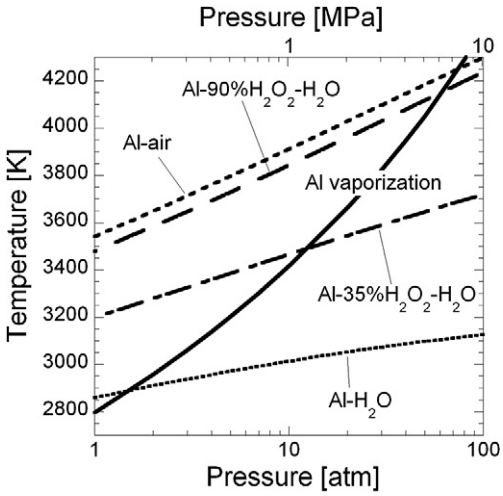

Fig. 1. Comparison of various adiabatic flame temperatures of stoichiometric Al combustion systems with Al vaporization temperatures over a range of pressure.

of primarily hydrogen (H_2) and aluminum oxide or alumina (Al_2O_3):

$$2Al_{(s)} + 3H_2O_{(l)} \rightarrow Al_2O_{3(s)} + 3H_{2(g)}$$
$$\Delta H_{R,\,298\,K} = -409 \text{ kJ per mole Al}, \quad (1)$$

$$4Al_{(s)} + 3H_2O_{2(l)} \rightarrow 2Al_2O_{3(s)} + 3H_{2(g)}$$
$$\Delta H_{R,\,298\,K} = -697 \text{ kJ per mole Al}. \quad (2)$$

In a study of the Al–$H_2O_{(l)}$ reaction and its applicability to space propulsion, it was shown that H_2O_2 addition would theoretically increase specific impulse (I_{sp}) as well [27]. Using the NASA Chemical Equilibrium Applications Program (CEA) [28], adiabatic flame temperatures of stoichiometric mixtures of Al with several oxidizers (consisting of air, $H_2O_{(l)}$, and H_2O_2 mixtures) were calculated as a function of pressure and compared to the Al vaporization temperature (Fig. 1). Over the entire range of pressures shown, the Al and air mixtures exhibited flame temperatures higher than the Al vaporization temperature, while the calculated Al–$H_2O_{(l)}$ mixture flame temperature is greater than the vaporization temperature only at pressures below approximately 1.5 atm. Based on single-particle Al combustion experiments by Bucher et al. [1], transitions in the combustion mechanisms may be expected to occur as flame temperatures are augmented with increasing H_2O_2 concentration, raising the adiabatic flame temperature above the aluminum vaporization temperature. More specifically, at flame temperatures below the vaporization temperature, the flame front may be considered to lie at the molten surface of the Al fuel, typical of heterogeneous surface reactions. As the vaporization temperature of the Al is exceeded, the reaction flame front is extended away from the particle surface, creating a gaseous diffusion reaction. It is important to note that the CEA calculations described do not include an oxide passivation layer, which would be present in any Al particle reaction, thus lowering adiabatic flame temperatures.

An interesting aspect of the aluminum, water, and hydrogen peroxide system is that regardless of the H_2O_2 concentration used in the oxidizer, under stoichiometric conditions, the primary reaction products formed are H_2 and Al_2O_3. The production of hydrogen (with heat) allows this combustion system to be applied in unique ways to various technologies. In most combustion systems, usable heat and work are obtained from the initial reaction process and the expansion of gaseous products, which are no longer used and are expelled to the surroundings. Due to the large amount of high-temperature H_2 produced from this simple combustion system, the gas products may be collected or immediately burned to increase the overall efficiency and energy release of the process. The H_2 generated allows this system to be used as a portable source of H_2 generation for various technologies such fuel cells. The system may well apply to various air-breathing and space propulsion systems as already mentioned, with or without further combustion of hot H_2.

The primary goal of this study was to characterize the burning process of nAl–$H_2O_{(l)}$–H_2O_2 mixtures. In particular, the effects of pressure, equivalence ratio, and H_2O_2 concentration in $H_2O_{(l)}$ solution were examined in terms of burning rates and chemical efficiencies. The results of this study will allow a better understanding of the combustion processes of simple heterogeneous combustion systems containing nAl and other metallic particles. It is also important to understand burning characteristics of systems such as this to recognize their applicability to propulsion and H_2 generation systems. The fundamentals learned from this reaction system also bridge our level of understanding of gas–solid combustion systems to more complex solid–solid nanoenergetic systems such as metastable intermolecular composite systems (MICs) [29–31].

2. Experimental methods

Two experiments were employed during this investigation. In order to determine linear and mass-burning rates, an optical pressure vessel of large volume was used to monitor the deflagration process in a quartz tube over time. A smaller closed bomb, which contained the combustion products after reactions, was used to determine chemical efficiencies. The aluminum particles, oxidizers, and sample prepa-

ration were identical, although the sample masses and loading procedures varied.

2.1. Materials and sample preparation

All experiments conducted during this investigation used aluminum particles with a nominal diameter of 38 nm, produced by Technanogy, with an active Al content of 54.3% by mass, provided by the manufacturer, and confirmed independently to be within experimental reproducibility using thermogravimetric analysis (TGA). The oxide layer thickness and specific surface area were reported to be 3.1 nm and 54.1 m^2/g, respectively, by the manufacturer. A pycnometer test determined particle density to be 3.205 g/cm^3, which is inclusive of the oxide passivation layer (~3.97 g/cm^3), which explains the difference from bulk aluminum (2.7 g/cm^3). A scanning electron microscopy (SEM) image of the particles is shown in Fig. 2. Given their small size, they are fairly spherical and have a relatively narrow size distribution. A more detailed particle characterization of similar Technanogy particles has been conducted by Mang et al. [32].

The nAl particles were mixed in small batches with unpurified distilled water and hydrogen peroxide solution (35 wt% in $H_2O_{(l)}$, Sigma-Aldrich, MW = 34.01, CAS Number 7722-84-1). Before each sample was mixed, the H_2O_2 solution was diluted to the desired H_2O_2 concentration using the distilled water. No attempt was made to refine the H_2O_2 solution to greater concentrations; therefore 35% was the highest concentration used in any test. All mixture weight measurements were accomplished using a Mettler-Toledo analytical balance (AB265-S) with a readability as low as 0.01 mg. The stoichiometry of each mixture was calculated based on the value of the active Al content supplied by the manufacturer. The stoichiometric oxidizer-to-fuel mass ratio is approximately 1, decreasing slightly with H_2O_2 concentration. Each sample was measured into and mixed in small polyethylene bags by hand for a minimum of 5 min or until all noticeable agglomerates were dispersed. Mixing times generally varied from 4 to 6 min. Stoichiometric mixtures become a slightly damp black powder after mixing, whereas under fuel-lean conditions, the mixture was wet and behaved as a thick clay mud. An image of these mixtures, as well as additional details of the experiments and procedures, may be found in a previous publication [14]. In all experiments, the fuel and oxidizer mixtures were mixed in small batches and promptly loaded into the desired experiment in order to avoid any oxidizer loss through vaporization or slow, low-temperature reactions.

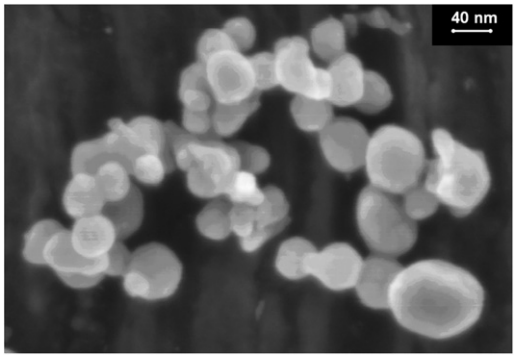

Fig. 2. SEM micrograph of Technanogy 38-nm aluminum particles (courtesy of Ed Roemer, Los Alamos National Laboratory).

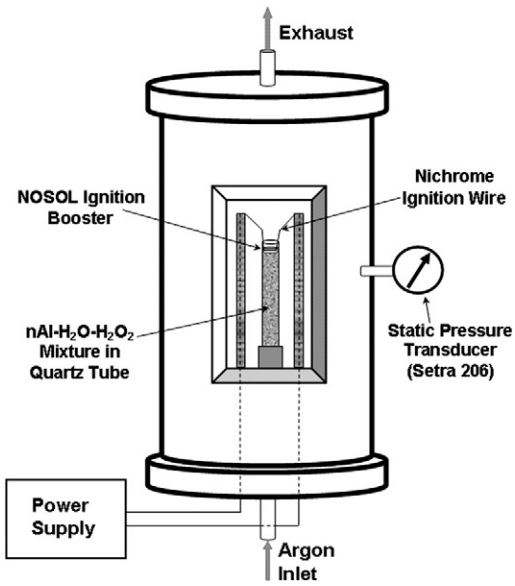

Fig. 3. Schematic of windowed pressure vessel used for burning rate measurements.

2.2. Burning rate measurements

The steady state linear and mass-burning rates of the nAl, $H_2O_{(l)}$, and H_2O_2 mixtures were acquired using a pressure vessel under well-controlled operating conditions in argon (Ar), shown schematically in Fig. 3. The vessel, constructed of stainless steel, is equipped with four optical viewing windows and has a total free volume of 23 L to minimize pressure variations due to gas evolution during the combustion process. Prior to ignition, the vessel was brought to the desired initial pressure by regulating the flow of Ar through inlet and exhaust valves. Once the desired pressure was reached, a continuous purge of Ar was maintained in order to prevent exhaust gases from obstructing the viewing windows. One of the

Table 1
Packing densities of various mixtures

Φ	Particle diameter (nm)	H_2O_2 (wt%)	Packing density (g/cm^3)
1.00	38	0	0.726 ± 0.028 [14]
1.00	38	10	0.662 ± 0.017
1.00	38	25	0.669 ± 0.017
1.00	38	35	0.673 ± 0.021
0.50	38	0	1.384 ± 0.030 [14]
0.67	38	0	1.478 ± 0.030 [14]
0.75	38	0	1.055 ± 0.018 [14]
1.25	38	0	0.731 ± 0.016 [14]

optical viewports of the chamber was used for real-time recording of the combustion process by a digital video camera, while the opposite viewport was used for backlighting the sample. Backlighting was accomplished using a single external light source that was optically diffused to distribute light evenly.

Using the procedure previously outlined, the fuel and oxidizer were mixed into the desired composition. Immediately after mixing, the sample was loaded into 10-mm-diameter (8-mm-I.D.) quartz tubes approximately 75 mm long. Each tube was closed off at one end using hot craft glue and a small amount of modeling clay. The mass and volume of each mixture were measured after the tube was loaded to determine the packing density (ρ). Table 1 displays the packing densities for various mixture compositions and their associated standard deviations. A small ignition booster, made of double-base gun propellant (NOSOL 363), threaded over a piece of Nichrome wire was placed on top of the loaded sample. The ends of the Nichrome wire were attached to wire leads, allowing a power supply to be connected via electrode feedthroughs after the strand assembly was loaded into the pressure vessel. Once the strand assembly was loaded, and all wire and gas connections were made, pressurization of the chamber was initiated. Chamber pressure was measured using a Setra 206 (0–5000 psig) pressure transducer. A Nicolet Genesis multichannel data acquisition system monitored and recorded the pressure transducer outputs as a function of time at a standard sampling rate of 1000 Hz. The luminous combustion wave was recorded using the digital video camera, allowing linear burning rates to be determined by tracking the position of the reaction front over time. Linear burning rates (r_b) were converted to mass burning rates per unit area ($m_b = \rho \times r_b$) in order to account for small variations in the packing densities [15].

2.3. Localized pressure measurements

To better characterize the burning of these mixtures, localized pressure measurements were conducted by drilling 1/32-inch-diameter holes into the quartz tubes, isolating them, and connecting a pressure transducer through small pressure taps. This was accomplished by mounting the tube into a specially machined stainless steel block, which allowed up to six fast-response dynamic pressure transducers (PCB Model 111A22) to be placed along the length of the tube at 1-cm intervals, shown in Fig. 4. To reduce errors in the pressure transducer output due to thermal shock, an extra sealing ring was used with the transducers to displace them an extra 0.015 in. (0.381 mm) from the sample tube. Room temperature vulcanizing (RTV) silicone was used as a barrier material between the hot combustion gases and the transducer face as well. In addition to these six pressure sensors, a seventh PCB transducer was used to monitor the changes in chamber pressure, in addition to the diaphragm Setra transducer. To ensure that the pressure transducers and tapped holes in the quartz tubes lined up correctly, a small alignment tab was created, which allowed the tubes to be aligned and fixed into position with a small set screw and then loaded with the nAl and oxidizer mixture separately. The Genesis data acquisition system was used as in the burning rate measurements, with sampling rates as high as 0.5 MHz.

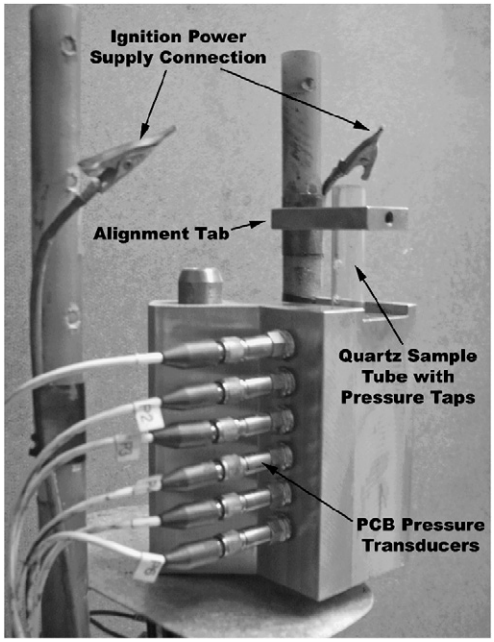

Fig. 4. Experimental setup used for localized pressure measurements (sample tube is shown partially removed from the steel block for viewing purposes).

2.4. Combustion efficiency measurements

Chemical combustion efficiencies were determined using a closed bomb chamber coupled to a gas

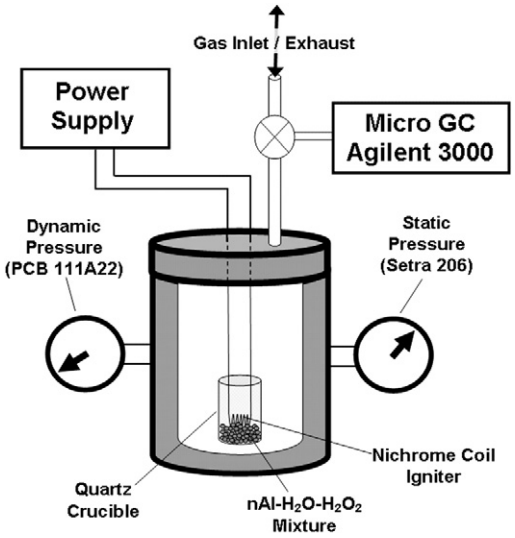

Fig. 5. Schematic of the closed bomb chamber coupled to a gas chromatograph.

chromatograph (GC), shown in Fig. 5. The chamber, constructed of stainless steel with a total free volume of 156 cm^3, is able to withstand pressures beyond 34 MPa. The chamber has multiple access ports to allow for pressure transducers, inlets, and exhausts, as well as feedthroughs for electrical connections. Static pressures were monitored using a Setra 206 pressure transducer, and a fast-response PCB transducer was utilized for dynamic measurements. Using the sample preparation guidelines described, the fuel and oxidizer mixture was loaded into a small quartz crucible, with a total free volume of 7 cm^3. In each experiment, roughly 1 g of mixture was used, to maintain consistency between tests. The crucible and sample were installed in the vessel using a small platform suspended from the lid of the chamber. A coiled Nichrome wire was also fitted into the crucible and connected to two separate electrode feedthroughs to serve as an ignition source. Once the chamber was assembled and sealed, it was purged with argon a minimum of three times to remove nitrogen and oxygen from the system. The Nicolet Genesis multichannel data acquisition system was used to monitor and record pressures at a sampling rate of 5 kHz.

To quantify the chemical efficiency of each test, an Agilent GC (MicroGC 3000) was used to measure the H_2 concentration in the combustion chamber after each sample was ignited and solid by-products were allowed to settle. The output from the GC was compared to a calibration curve to determine the volumetric concentration of the H_2 present in the chamber ($[H_2]_{meas}$). The calibration curve was created by sampling from a specified flow of Ar and H_2 regulated using two Teledyne Hastings 200 Series mass flow controllers. The overall chemical efficiency, η_{chem}, was calculated using the ratio of the measured H_2 to the maximum theoretical H_2 formed from the combustion reaction ($\eta_{chem} = [H_2]_{meas}/[H_2]_{theor}$).

The maximum theoretical H_2 concentration in the chamber after combustion is based on the amount of Ar used to pressurize the chamber prior to testing, as well as the masses of the various mixture constituents (Al, Al_2O_3, H_2O, and H_2O_2). The primary assumption of the theoretical calculation is that the combustion reaction is complete with no dissociation, leaving only H_2 in the gas phase, and all other product species (Al, Al_2O_3, H_2O, etc.) in liquid or solid form. Any water vapor that may be present is neglected. Due to the small sample mass used during testing and the short combustion times, these assumptions are justified, as the system is cooled to nearly room temperature by the time sampling takes place, solidifying the alumina, condensing any steam present, and recombining available H atoms to H_2. Note that equilibrium calculations show that no more than approximately 1% H_2O (molar) is formed during combustion.

Using the assumptions mentioned, the maximum theoretical H_2 concentration was found by initially determining the amount of Ar present in the chamber prior to combustion. This was achieved using the pressure (P) and temperature (T) of the Ar gas, as well as the free volume (V) of the test chamber. The pressure was known from the static pressure transducer output, while the temperature in the chamber was assumed to be in equilibrium with the surroundings, allowing temperature to be monitored externally. The free volume of the chamber was also carefully determined, taking into account all volumes displaced or added due to the crucible, feedthroughs, valves, supports, etc. Since the Ar was at room temperature (21–24 °C), at high pressures the compressibility factor (Z) of the Ar gas is reduced, creating calculated Ar mass inconsistencies of greater than 5% ($Z = 0.945$ at 2000 psia) between ideal gas theory and tabulated data, as reported by the National Institute of Standards and Technology (NIST). Due to these differences, NIST database software (NIST12, an abbreviated version of NIST REFPROP) [33] was used to determine the Ar densities, and therefore masses, for all theoretical chemical efficiencies.

The amounts of nAl and liquid oxidizers used in each run were directly calculated during the mixing process using the analytical balance, assuming an active Al particle content of 54.3%, no evaporation of liquid oxidizers, and uniform mixing. With the exact masses of the reactants known, a maximum H_2 production could be determined. With the assumption that H_2 and Ar are the only gas phase species present in the chamber after combustion, calculation of the

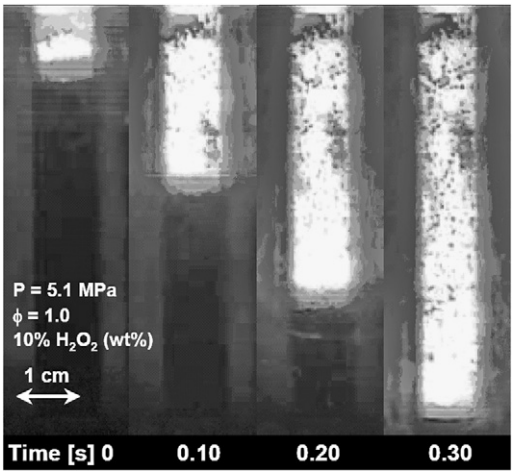

Fig. 6. Captured images of the normal deflagration process of a nAl–H_2O–H_2O_2 mixture.

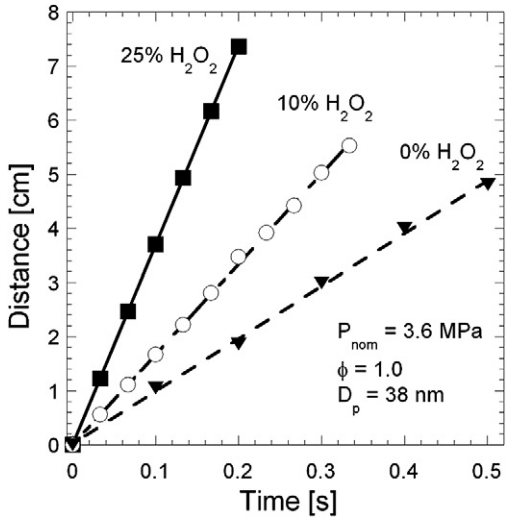

Fig. 7. Trajectory plots of typical deflagrations with varying H_2O_2 concentrations.

theoretical H_2 concentration ($[H_2]_{theor}$) is straightforward.

3. Results and discussion

The linear burning rates were determined by measuring the combustion wave front propagation from recorded video. Fig. 6 illustrates a typical combustion process within the quartz sample tube using a stoichiometric mixture of nAl, $H_2O_{(l)}$, and 10% H_2O_2. The image of the normal deflagration shows that a steady, flat reaction front is obtained shortly after ignition. The flame front is shown to exist at the surface of the reactant mixture, indicative of a heterogeneous surface ignition and reaction. The extremely luminous region above the wave front is molten alumina (Al_2O_3) radiating at a high temperature. Fig. 7 shows a trajectory plot (distance vs time) of stoichiometric mixtures with different H_2O_2 concentrations, exemplifying that nearly steady state deflagrations occur, as evident from the linearity of the data. These figures indicate, at least from a macroscopic perspective, that packing densities and reactant mixing are fairly uniform within the tube. The trajectory plot also shows the effect of H_2O_2 concentration on the burning rates, substantially increasing the rate of reaction with increasing concentration. In a previous study of nAl and liquid water mixtures, a significant amount of the alumina formed during the reaction remained in the tube for the slow-burning-rate mixtures [11,14]. In the current study, the addition of H_2O_2, excluding very lean conditions, caused the majority of the molten alumina to be carried out the top of the tube by the generated H_2 flow and condense in the pressure vessel, leaving only the walls of the quartz tubes coated with alumina.

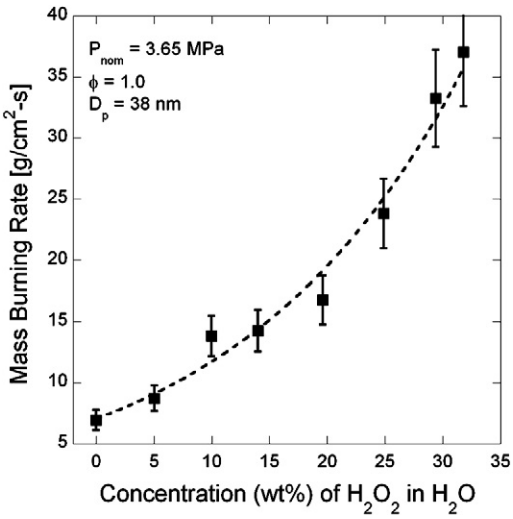

Fig. 8. Effect of H_2O_2 concentration on the mass burning rate per unit area.

Using the captured video images, the linear and mass-burning rates were determined as functions of the H_2O_2 concentration under nearly constant-pressure conditions (~3.65 MPa). Using the mixture packing densities, the mass-burning rates per unit area were determined from the linear burning rates (Fig. 8). The H_2O_2 concentration is observed to have a dramatic effect on the combustion process, increasing the mass-burning rate per unit area by more than a factor of 5 from 0 to 32% H_2O_2. Both the linear and mass-burning rates appear to increase exponentially

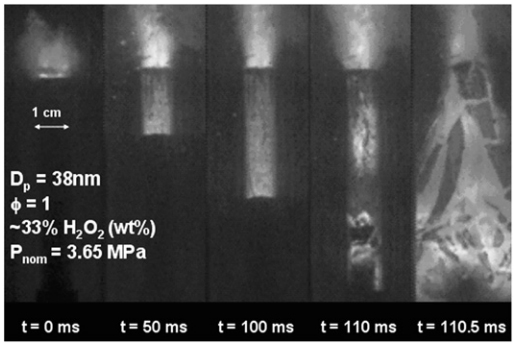

Fig. 9. Captured high-speed camera images of the combustion wave progress of a nAl–H_2O–H_2O_2 mixture.

with H_2O_2 concentration. Burning rates were not determined at higher concentrations due to a change in burning behavior at higher concentrations. Captured images from a high-speed digital video camera (Vision Research Phantom v5.3) of one of these cases (33% H_2O_2 and 3.65 MPa) are presented in Fig. 9. Notice that shortly after ignition the combustion wavefront appears to propagate steadily in a normal or layer-by-layer mode, as typically found at lower concentrations. However, approximately two-thirds the way down the tube, the wavefront jumps forward by "fingering" or "jetting" through the bed, causing the tube to rupture due to overpressurization. This anomalous burning phenomenon was observed not only in the quartz tubes, but also in wax paper tubes, where much of the walls are consumed near the luminous front, eliminating chances of confinement or pressure increases due to condensed phase product buildup. The change in the deflagration process has some indications of a transition between normal deflagration, or conduction-heat-transfer-dominated combustion, to convective burning, which is described as the breakdown of normal surface burning of a gas-permeable system as a result of penetration of combustion products into the reactant bed [34], or a deflagration wave whose propagation rate is controlled by convection via rapid penetration of hot gases [35]. However, there is one main characteristic of these mixtures that does not match previously reported conditions of convective burning of solid combustibles. At high H_2O_2 concentrations ($> \sim$33%) and low pressures (slightly above 1 atm), which demonstrate rather low burning rates prior to tube rupture compared to lower H_2O_2 concentrations at high pressure, the anomalous burning phenomenon is also observed, causing tube rupture. With 25% H_2O_2 concentrations, relatively high burning rates could be obtained at high pressures (39.4 cm/s at 13.0 MPa, $\Phi = 1$) without overpressurization. This indicates that the chemical makeup of the reactant mixture, i.e., the H_2O_2 concentration, plays the dominant role in transition in

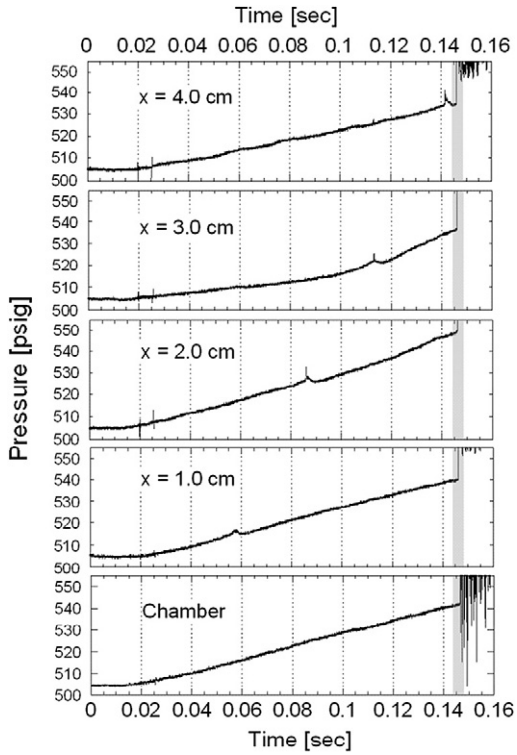

Fig. 10. Localized pressure measurements during the combustion of a stoichiometric mixture with 33% H_2O_2.

combustion dynamics, as opposed to burning rate and pressure, which is most often used to characterize the transition to convective burning in granular solid propellants and explosives. As a caveat, mixtures of the nAl powders with high concentrations of hydrogen peroxide appeared fairly sensitive to ignition and reacted quickly in open air, making them potentially very dangerous, even in small quantities.

To further investigate the combustion process at high H_2O_2 concentrations, pressure measurements along the length of the tube during burning were made. It was hypothesized that at high H_2O_2 concentrations the pressure may locally increase at the flame front as a result of exhaust gases being choked by alumina accumulation within the tube, reactant decomposition in the preheat zone of the combustion wave, or compaction of the particle bed, causing the propagation mechanism to transition. Fig. 10 shows the pressure measurements at various locations along the sample tube for an experiment in which overpressurization did occur. Also shown is the chamber pressure, which increases steadily during the combustion process due to the gas evolution from the reaction. Notice that the localized pressure measurements all increase at roughly the same rate as the chamber pressure prior to the overpressurization, which is shaded in Fig. 10. A magnified view of the overpressurization is shown

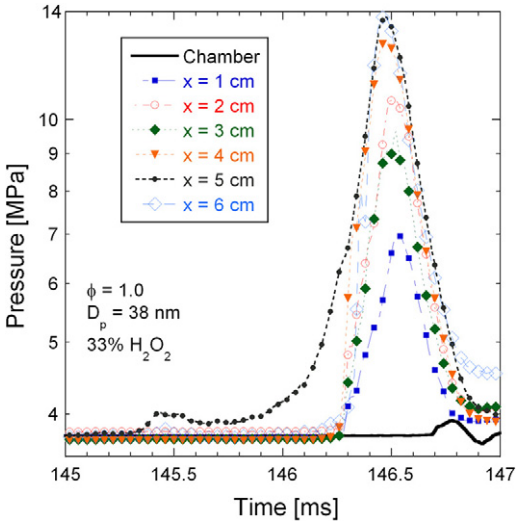

Fig. 11. Localized pressure measurements during an overpressurization of the quartz sample tubes.

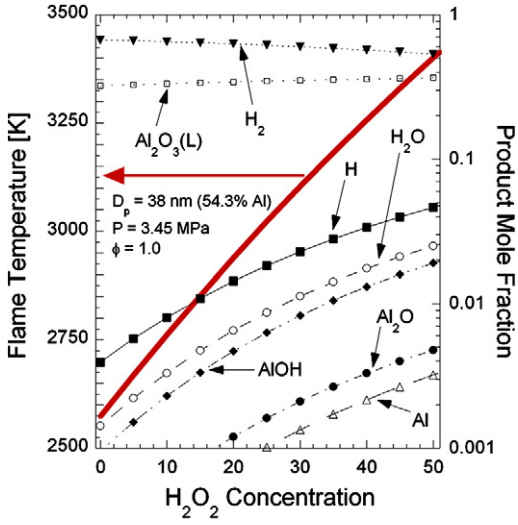

Fig. 12. Equilibrium calculations of the product mole fractions and adiabatic flame temperatures at varying H_2O_2 concentration.

in Fig. 11. From Fig. 10 the position of the combustion wave front as it propagates down the tube may be located from small pressure spikes (<10 psi) at 1, 2, 3, and 4 cm down the tube. The burning rate deduced from the spike locations is essentially the same rate as obtained from the photographic burning rate results, and the process is practically constant-pressure, since the pressure deviation of the spikes is only a small percentage of the system pressure. These results indicate that prior to the overpressurization the burning process is progressing in a normal manner. The results of Fig. 11 show that there is a small peak in pressure at the fifth pressure transducer, just prior to the overpressurization, where momentary pressures greater than 13.5 MPa are observed. The combustion wave was somewhere between the fifth and sixth transducers when the process changed dramatically. This is determined because of the small peak at the fifth port, followed less than a millisecond later by the overpressurization, for which the maximum pressures are seen at the fifth and sixth transducers. Peak pressures decreased with distance from the bottom two pressure taps of the tube, further indicating that the overpressurization occurs in the lower part of the tube. Meanwhile, the chamber pressure was relatively unaffected.

In order to understand the thermodynamic influence of the increased H_2O_2 concentration on the combustion process, equilibrium calculations were performed using the NASA CEA program. These calculations accounted for the use of 38-nm Al particles and an active aluminum content of 54.3% by incorporating the alumina into the reactant mixture. Fig. 12 illustrates the influence of the H_2O_2 concentration on the adiabatic flame temperature as well as the primary product mole fractions. From the figure, the flame temperature increases by approximately 600 K from 0 to 35% H_2O_2 for stoichiometric conditions. Comparing Fig. 12 to Fig. 1, the influence of inert Al_2O_3 addition reduces the flame temperature more than 150 K at 35% H_2O_2. In terms of the combustion products formed, the primary final products are H_2 and Al_2O_3, as expected. Alumina is present prior to the reaction as the Al particle passivation layer, and is formed during the fast Al oxidation process of the combustion reaction. Under stoichiometric conditions, the alumina is roughly 30% by mass of the reactant mixture when the 54.3% active Al particles are used under all H_2O_2 concentrations. This alumina is essentially a heat sink and diffusion barrier, undergoing phase changes during the combustion process, and reducing the maximum reaction temperatures. This further emphasizes why even small reductions in this inert layer, while maintaining particle passivation for sensitivity and storage concerns, would make a large contribution to the propulsion, power, and explosives community. A more interesting point concerning the presence of the oxide layer is that the mixture temperature lies below the Al vaporization temperature (~3870 K at 3.65 MPa, from Fig. 1). In the homogeneous limit of mixed reactants, this temperature implies that the combustion process would be heterogeneous, and not the vapor-phase combustion more typical of large-diameter Al particles in air, where a diffusion flame encompasses the particle. Hydrogen, the second of the two primary combustion products, is maintained at relatively the same level over the range of H_2O_2 concentrations consid-

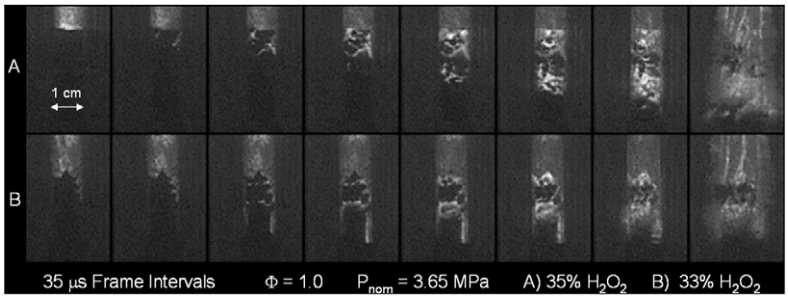

Fig. 13. Captured high-speed video images of combustion wave transitions at high H_2O_2 concentrations.

ered, decreasing only slightly. The small reduction of H_2 produced with increasing H_2O_2 is explained by the increased addition of Al into the reactant mixture to maintain stoichiometry. The increased flame temperatures also increase the amount of dissociation, i.e., primarily H_2 molecules dissociating to H atoms. However, the majority of the H atoms produced most certainly recombine to form H_2 or H_2O if the products are allowed to cool. In terms of the transition to convective burning found at high H_2O_2 concentrations, the information ascertained from the equilibrium calculations does not point to a specific change in the system leading to the overpressurization of the sample tubes. However, the equilibrium calculations assume a homogeneous reactant mixture, which does not describe the actual reactants correctly. In reality, localized reactions may produce large concentrations of nonequilibrium species as well as flame temperatures greater than equilibrium conditions over the course of the combustion process.

The addition of H_2O_2 was examined in more detail by considering its decomposition process alone, and how it may couple with aluminum combustion. Hydrogen peroxide is known to undergo an exothermic decomposition process, forming water vapor and molecular oxygen products, with primary intermediate radical species of OH and HO_2. Equilibrium calculations indicate that this decomposition process can increase the reactant bed temperature more than 150 K at higher H_2O_2 concentrations and pressures; however, these temperatures are well below the predicted ignition temperature of the 38-nm particles (i.e., ∼750 K, based on DSC-TGA measurements). Additionally, the homogeneous H_2O_2 decomposition process is rather slow at lower temperatures. However, previous studies indicate that H_2O_2 decomposition rates may be greatly increased by using a heterogeneous catalysis process. A recent study has shown increased liquid H_2O_2 decomposition rates in the presence of water and alumina particles [36]. The vapor phase decomposition process is known to be heterogeneously catalyzed in the presence of aluminum oxide as well [37]; both processes show an oxide surface area (i.e., active area) dependence. Based on the results of these studies, the presence of the water and the high-surface-area Al_2O_3 and Al particles increases the decomposition rates of hydrogen peroxide, forming O_2 as well as OH and HO_2 radicals. The partial pressure of these gas phase species is dependent on the initial H_2O_2 concentration alone, and is independent of system pressure. The production of these species, which have much faster oxidation kinetics than water vapor, increases reaction rates, reduces flame thickness, and may create localized "hot spots" within the reactant mixture. The surface-catalyzed decomposition of hydrogen peroxide also increases localized pressure, as 1.5 gas phase moles (i.e., $H_2O + 0.5O_2$) are formed per mole of H_2O_2. These factors allow for the transition in the combustion process.

Based on the results from the high-speed videos, the localized pressure measurements, and the thermochemical studies of H_2O_2, it is believed that the transition in the combustion process is due to a combination of decomposition (particularly of H_2O_2, due to the apparent critical concentration) and the compaction of the reactant bed, which creates a gap between the bed and the tube wall large enough for wave propagation. Analysis of the high-speed videos shows that in the cases of tube rupture the combustion wave stalls or slows momentarily, which is not seen with the standard video camera (see Fig. 13). The stalling process indicates that the bed is compacting, increasing in density, or that a heat sink is encountered, such as increased phase transformation in the reactant bed. Shortly after stalling, the video shows the wave moving along the walls of the tube very quickly and then propagating into the bed through cracks. This flame spreading and fingering down the tube walls and into cracks greatly increases the surface area of burning, which quickly generates enough gas to overpressurize and shatter the tube.

Further characterization of the Al–H_2O–H_2O_2 mixtures was accomplished by examining the effects of the pressure and overall mixture equivalence ratio on burning rates. Fig. 14 illustrates the effect of

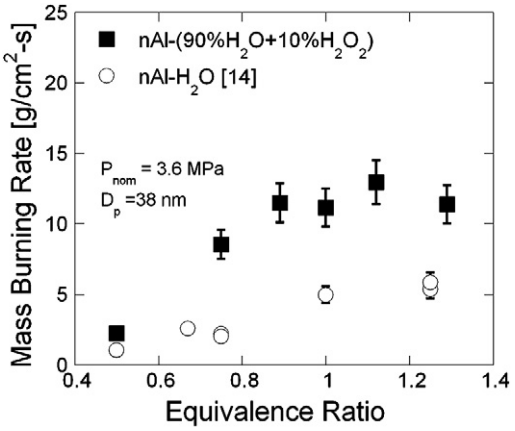

Fig. 14. Effect of equivalence ratio on mass burning rate per unit area.

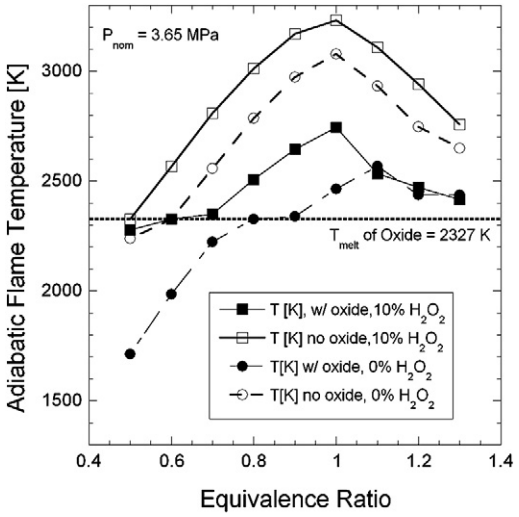

Fig. 15. Equilibrium flame temperatures of 38 nm Al–H_2O mixtures with and without H_2O_2 (compared to the alumina melting temperature).

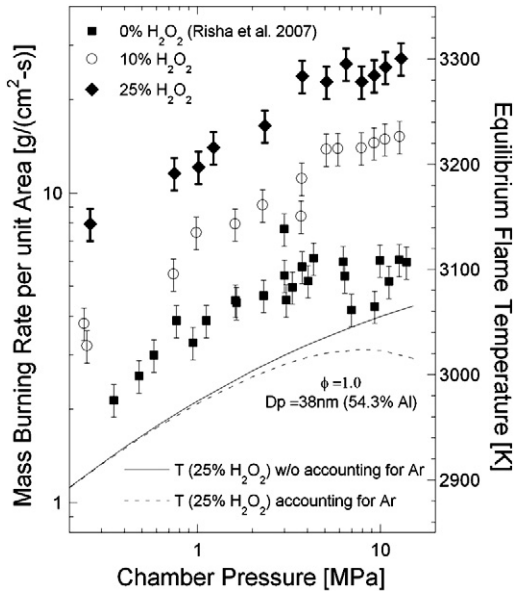

Fig. 16. Effect of pressure on mass burning rate per unit area and equilibrium flame temperature under stoichiometric conditions.

Φ on the mass-burning rate using an aqueous oxidizer solution of 10% H_2O_2 at a nominal pressure of 3.6 MPa. For comparison, burning rates of mixtures containing no H_2O_2, reported by Risha et al. [15] are shown as well. The figure demonstrates that the mixture containing H_2O_2 reacts to changes in Φ similarly to the mixture without H_2O_2. As in the pure H_2O mixtures, slightly fuel-rich mixtures appear to burn as fast as or faster than the stoichiometric mixtures. For the mixtures containing 10% H_2O_2, the highest burning rate occurred at $\Phi = 1.13$. For lean mixtures, the burning rate drops off rapidly below Φ of 0.75. It is interesting to note that under very lean conditions, the burning rates of both mixtures (with and without H_2O_2) are nearly the same. Equilibrium flame temperatures were calculated using CEA and are shown in Fig. 15 for varying equivalence ratios. Also shown in the figure are the effects of the oxide passivation layer, further illustrating the reduction in flame temperature. Noteworthy is the effect of the alumina creating the unique-shaped temperature profiles, in which the flame temperature is strongly correlated with the melting temperature of the oxide under fuel-lean and -rich conditions. Furthermore, for overall Φ of less than approximately 0.6 and 0.8 for 10% and 0% H_2O_2, respectively, the mixture temperature is less than the oxide melting temperature. This condition could suggest that oxidation of the Al particles within the oxide shell is not promoted by melting of the oxide layer, but by damage to the shell from thermal or mechanical stresses, such as Al melting. However, since the mixture is quasi-homogeneous, local regions of higher temperature likely occur and the oxide may melt.

The effects of pressure on the overall mixture burning rates are shown in Figs. 16 and 17. Fig. 16 illustrates the mass-burning rates for three separate stoichiometric mixture compositions (0, 10, and 25% H_2O_2) over a range of pressures from slightly above atmospheric pressure up to 12.4 MPa. Clearly demonstrated is that the addition of H_2O_2 to the nAl–$H_2O_{(l)}$ mixtures greatly increases energy release and therefore increases the burning rate over a large pressure range. Although burning rates are increased, all the mixtures exhibit nearly the same pressure dependence. In the three cases shown, burning rates begin to become independent of pressure at levels above

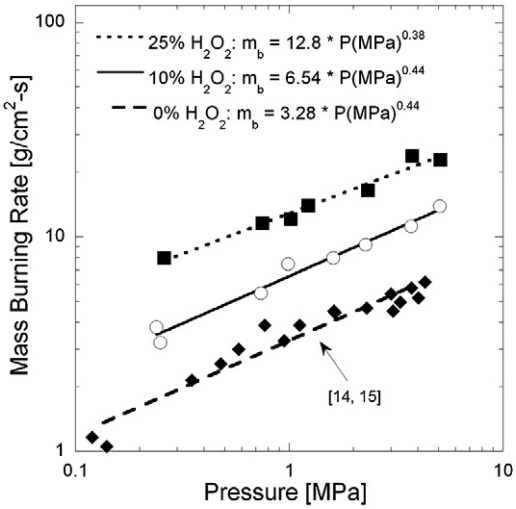

Fig. 17. Pressure dependence and burning rate formulas of stoichiometric mixtures of 0, 10, and 25% H_2O_2.

approximately 5 MPa. This transition in pressure dependence is explained by the void space in the packed mixture, which becomes progressively more occupied by argon as pressure is increased, acting a heat sink or diluent in the reactant mixture [15]. The affect of argon as a diluent is illustrated by the temperature curves in Fig. 16. Using the average packing density of the 25% H_2O_2 stoichiometric mixtures (36% of maximum theoretical), the void space and equilibrium flame temperatures were computed. As in the earlier work, this flame temperature reduction corresponds directly to the change in the pressure dependence of the linear and mass burning rates.

Fig. 17 displays the pressure dependence of the same three mixtures up to 5 MPa. From the pressure exponents in the burning-rate formulas, it is shown that all three mixtures exhibit similar pressure dependencies. The low exponents (near 0.5) suggest an overall first-order chemical reaction process ($\rho \times r_b = m_b \propto P^{n/2}$). Equilibrium calculations were also performed as a function of initial pressure. The results indicated an increase in temperature with increasing pressure (Fig. 1), with the reaction products being relatively unaffected, except for reductions in radical formation.

Chemical efficiencies were determined using the closed bomb (Table 2). Uncertainties in the efficiencies are also shown, determined by the propagation-of-error equation accounting for standard deviation in GC sampling and calibration, as well as the uncertainty in test measurements, such as pressure, mass, and temperature. Only select efficiencies are reported, since the overall efficiencies did not vary substantially over the entire pressure and H_2O_2 concentration ranges considered. In previous studies without

Table 2
Chemical efficiencies for stoichiometric nAl–H_2O–H_2O_2 mixtures

Particle diameter (nm)	H_2O_2 (wt%)	Pressure (MPa)	Chemical efficiency (%)
38	0	3.48	96.8 ± 2.5
38	5	3.65	88.9 ± 5.9
38	10	3.33	93.1 ± 8.1
38	20	3.23	97.6 ± 6.3
38	30	3.35	96.6 ± 4.7
38	35	3.48	101 ± 2.5
38	10	0.45	96.3 ± 3.8
38	10	0.74	94.5 ± 3.5
38	10	2.10	96.3 ± 5.1
38	10	4.96	94.0 ± 4.6
38	10	7.54	100 ± 11.6
38	10	8.80	101 ± 7.5

H_2O_2 [15], chemical efficiency was found to vary with particle diameter, and not significantly with pressure, displaying only a very small dependence, except for pressures near 1 atm. The slight pressure dependence is illustrated in the table. Since 38-nm particles were used in this study, compared to the 80 and 130 nm of [15], all efficiencies were generally within 10% of the theoretical maximum, regardless of the H_2O_2 addition, indicating that combustion temperatures are high enough to reduce reaction times and oxidize nearly the entire Al particle. Since larger particles are preferable for H_2 generation due to the greater active Al content (and hence greater gravimetric and volumetric H_2 densities are possible), H_2O_2 addition to mixtures containing larger particles, or bimodal distributions of particles, may be a means to increase chemical efficiencies compared to the pure H_2O oxidizing systems. Additions of high-hydrogen-content compounds such as metal hydrides or borohydrides to Al–H_2O mixtures have also been considered to increase H_2 generation yields [12].

As with strand burning rate measurements, interesting observations were also made at high H_2O_2 concentrations in the closed-bomb experiments. Using 35% H_2O_2 concentrations, the quartz crucibles used to hold the reactants would shatter during the combustion process. Unlike the burning-rate experiments where the mixtures were packed tightly into narrow quartz tubes, the reactants in the chemical efficiency tests were less confined, given that the crucibles had 0.75-in. inside diameters and the reactants were not packed. Additionally, depending on the H_2O_2 concentration used, the visual appearance of the condensed phase reaction products changed. At lower concentrations, the product either caked onto the upper surface of the cell or fell to the bottom as particles with diameters on the order of a millimeter. The products caked onto the top of the chamber

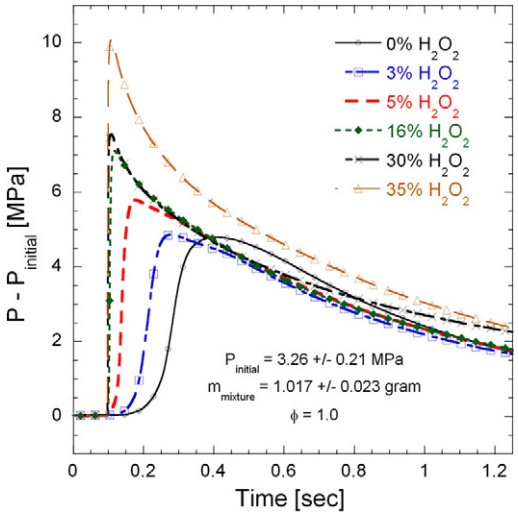

Fig. 18. Pressure vs time profiles of closed bomb tests using stoichiometric nAl–H_2O–H_2O_2 mixtures.

were white, except for the surface contacting the cell, which was grayish in color, suggesting that some of the products were quenched prior to complete oxidation. Many of the particles formed also displayed some grayish coloring as well. As H_2O_2 concentrations increased, product particle size was reduced, and at very high concentrations (>30%), the majority of product formation consisted of a fine white powder that coated much of the internal cell components. These trends also suggest that at the highest H_2O_2 concentrations, much of the aluminum burns in the vapor phase, yielding nanoaluminum oxide particles that formed during a gas phase condensation process.

Pressure profiles within the closed bomb as a function of the H_2O_2 concentration and time are shown in Fig. 18. The addition of H_2O_2 is shown to increase the initial pressurization rates and peak pressures, consequently reducing ignition delay times. At the highest H_2O_2 concentration shown, the induction period appears almost nonexistent, as the pressure spikes abruptly compared to the nAl–H_2O mixture. In the previous study by Risha et al. [11,15], using the identical experimental setup, it was found that at elevated pressures, the initial pressurization rate was nearly constant, while at atmospheric pressure, the pressurization rate was orders of magnitude lower, most likely due to the lower reaction rates and smaller heat losses to the surroundings.

4. Conclusions

The combustion of nanoaluminum, liquid water, and hydrogen peroxide has been characterized for a broad range of pressures, equivalence ratios, and concentrations of H_2O_2. This work has extended previous studies, which considered solely the nAl–liquid water system and explored a range of particle sizes. The major conclusions of this work are as follows:

1. The addition of H_2O_2 to quasi-homogeneous mixtures of nAl and liquid H_2O significantly increases combustion heat release, flame temperatures, and linear and mass-burning rates. At 3.65 MPa, linear and mass-burning rates increased by more than a factor of 5 between 0 and 32% H_2O_2.
2. Mass-burning rate pressure exponents of 0.44 and 0.38 were obtained for stoichiometric mixtures of nAl and liquid H_2O containing 10% and 25% H_2O_2, respectively, which is nearly the same value found for the pure H_2O system. From simple flame theory, the apparent pressure exponents suggest a first-order overall reaction processes, since the exponents are close to 0.5. Pressure dependence of the mass-burning rates for the 38-nm aluminum particles is lost above approximately 5 MPa, an effect of the void space in the reactant mixture, which is pressurized with argon, acting as a heat sink.
3. The burning rates and adiabatic flame temperatures strongly depend on Φ, particularly in the fuel lean regime. The largest burning rates occurred at a Φ slightly greater than 1.0 for a mixture with 10% H_2O_2 oxidizer concentration.
4. Equilibrium calculations show that the adiabatic flame temperatures are significantly affected by the H_2O_2 concentration of the reactant mixture, the pressure, the amount of oxide coating the particles, and the diluent gas filling voids in the reactant mixture. Increases in system pressure and H_2O_2 content increase temperatures significantly, while the alumina passivation layer may decrease the flame temperatures by more than 500 K, depending on the mixture composition and active Al content of the particles. At high pressures, burning rates may be suppressed due to pressurization of interstitial spaces in the reactant bed with inert gases, which lowers flame temperatures.
5. Above approximately 32% H_2O_2, anomalous burning of the reactant mixture is observed, causing the quartz strands to overpressurize and rupture. This phenomenon was observed at low pressures (∼2 atm), indicating an apparent critical H_2O_2 concentration, as opposed to a critical pressure, which implies that aluminum oxidation by H_2O_2 and its decomposition species (i.e., O_2, OH, HO_2) is driving the reaction into cracks in the reactant bed.

6. Chemical efficiencies of stoichiometric mixtures of 38-nm Al particles with $H_2O_{(l)}$ and H_2O_2 are generally greater than 90% and approach the theoretical maximum at high pressures and H_2O_2 concentrations.
7. Increased H_2O_2 concentration of the oxidizing solution reduces ignition delay times, increasing reaction and pressurization rates.

Acknowledgments

This work was sponsored by the U.S. Army Research Office under the Multi-university Research Initiative under Contract W911NF-04-1-0178. The support and encouragement provided by Ralph A. Anthenien is gratefully acknowledged. S.F.S. and B.C.T. were supported by the Joint Munitions Program (DoD/DOE) at the Los Alamos National Laboratory (LANL), which was formally operated by the University of California for the U.S. Department of Energy under Contract W-7405-ENG-36. The authors thank the personnel at LANL, specifically Ed Roemer for the SEM micrographs of particles, and Eric Sanders for supplying the aluminum particles.

References

[1] P. Bucher, R.A. Yetter, F.L. Dryer, T.P. Parr, D.M. Hanson-Parr, Combust. Flame 117 (1998) 351–361.
[2] M.W. Beckstead, Combust. Explos. Shock Waves 41 (5) (2005) 533–546.
[3] M.W. Beckstead, Y. Liang, K.V. Pudduppakkam, Combust. Explos. Shock Waves 41 (6) (2005) 622–638.
[4] N. Glumac, H. Krier, T. Bazyn, R. Eyer, Combust. Sci. Technol. 177 (2005) 485–511.
[5] S.E. Olsen, M.W. Beckstead, J. Propuls. Power 12 (4) (1996) 662–671.
[6] W. Vedder, D.A. Vermilyea, Trans. Faraday Soc. 65 (1969) 561–584.
[7] V.G. Ivanov, S.N. Leonov, G.L. Savinov, O.V. Gavrilyuk, O.V. Glazkov, Combust. Explos. Shock Waves 30 (4) (1994) 569–570.
[8] V.G. Ivanov, O.V. Gavrilyuk, O.V. Glazkov, M.N. Safronov, Combust. Explos. Shock Waves 36 (2) (2000) 213–219.
[9] T.F. Miller, J.D. Herr, in: 40th AIAA/ASME/SAE/ASEE Joint Propulsion Conference and Exhibit, Fort Lauderdale, FL, 2004.
[10] E. Shafirovich, V. Diakov, A. Varma, Combust. Flame 144 (2006) 415–418.
[11] G.A. Risha, S.F. Son, B.C. Tappan, V. Yang, R.A. Yetter, in: 33rd IPS Seminar, Fort Collins, CO, 2006, pp. 103–112.
[12] E. Shafirovich, V. Diakov, A. Varma, in: 44th AIAA Aerospace Sciences Meeting and Exhibit, Reno, NV, 2006.
[13] G.A. Risha, Y. Huang, R.A. Yetter, S.F. Son, V. Yang, B. Tappan, in: 44th AIAA Aerospace Sciences Meeting and Exhibit, Reno, NV, 2006.
[14] G.A. Risha, S.F. Son, R.A. Yetter, V. Yang, B.C. Tappan, Proc. Combust. Inst. 31 (2007) 2029–2036.
[15] G.A. Risha, J.L. Sabourin, S.F. Son, B. Tappan, V. Yang, R.A. Yetter, Combust. Sci. Technol. (2008), in press.
[16] T.J. Foley, C.E. Johnson, K.T. Higa, Chem. Mater. 17 (2005) 4086–4091.
[17] R.J. Jouet, A.D. Warren, D.M. Rosenberg, V.J. Bellitto, P. Kihong, M.R. Zachariah, Chem. Mater. 17 (2005) 2987–2996.
[18] A. Gromov, A. Ilyin, U. Forter-Barth, U. Teipel, Propell. Explos. Pyrotech. 31 (5) (2006) 401–409.
[19] A.A. Gromov, U. Forter-Barth, U. Teipel, Powder Technol. 164 (2006) 111–115.
[20] B.Z. Eapen, V.K. Hoffmann, M. Schoenitz, E.L. Dreizin, Combust. Sci. Technol. 176 (2004) 1055–1069.
[21] W.C. Schumb, C.N. Satterfield, R.L. Wentworth, Hydrogen Peroxide, Reinhold, New York, 1955.
[22] G.E. Moore, K. Berman, Jet Propuls. 26 (11) (1965) 965–968.
[23] R.V. Osmon, Chem. Eng. Prog. Symp. Ser. 62 (61) (1966) 92–102.
[24] M.C. Ventura, S.D. Heister, J. Propuls. Power 11 (3) (1995) 562–565.
[25] E.J. Wernimont, S.D. Heister, J. Propuls. Power 16 (2) (2000) 318–326.
[26] D. Andrews, J. Brit. Interplan. Soc. 43 (1990) 319–328.
[27] A. Ingenito, C. Bruno, J. Propuls. Power 20 (6) (2004) 1056–1063.
[28] B.J. McBride, S. Gordon, Computer Program for Calculation of Complex Chemical Equilibrium Compositions and Applications, NASA, 1996.
[29] B.W. Asay, S.F. Son, J.R. Busse, D.M. Oschwald, Propell. Explos. Pyrotech. 29 (4) (2004) 216–219.
[30] W.L. Perry, B.L. Smith, C.J. Bulian, J.R. Busse, C.S. Macomber, R.C. Dye, S.F. Son, Propell. Explos. Pyrotech. 29 (2) (2004) 99–105.
[31] J.J. Granier, M.L. Pantoya, Combust. Flame 138 (2004) 373–383.
[32] M.T. Mang, R.P. Hjelm, S.F. Son, P.D. Peterson, B.S. Jorgensen, Report No. LA-UR-06-3251, Los Alamos National Laboratory, Los Alamos, NM, 2006.
[33] E.W. Lemmon, M.O. McLinden, M.L. Huber, NIST Standard Reference Database 12, 5.2, 2005.
[34] A.F. Belyaev, A.I. Korotkov, A.A. Sulimov, Combust. Explos. Shock Waves 2 (3) (1966) 28–34.
[35] B.W. Asay, S.F. Son, J.B. Bdzil, Int. J. Multiphase Flow 22 (5) (1996) 923–952.
[36] A. Hiroki, J.A. Laverne, J. Phys. Chem. B 109 (8) (2005) 3364–3370.
[37] A.Z. Arutyunyan, G.L. Grigoryan, A.B. Nalbandyan, Kinet. Katal. 27 (6) (1986) 1173–1178.